AN ABSTRACT OF THE THESIS OF

Richard Allen Nixon (Name) for the M. S. (Degree) in Chemistry (Major)

Date thesis is presented [illegible]

Title CHRONOPOTENTIOMETRY OF Sm(III) AND Pm(III) IN MOLTEN LiCl-KCl EUTECTIC

Abstract approved [redacted] (Major professor)

Samarium (III) and promethium (III) were studied by chronopotentiometry in a molten LiCl-KCl eutectic. Tungsten electrodes were used to avoid alloying effects encountered with platinum electrodes. Adsorption phenomena were observed which prevented the study of any kinetic effects. The quarter wave potentials were measured as: Sm(III) = 0.95 ± 0.05 volts, Pm(III) = 1.21 ± 0.06 volts. The diffusion coefficients were calculated to be: Sm(III) = 2.5×10^{-6} ± 0.3 cm^2/sec, and Pm(III) = 2.2×10^{-6} ± 0.3 cm^2/sec.

CHRONOPOTENTIOMETRY OF Sm(III) AND Pm(III) IN MOLTEN LiCl-KCl EUTECTIC

by

RICHARD ALLEN NIXON

A THESIS

submitted to

OREGON STATE UNIVERSITY

in partial fulfillment of
the requirements for the
degree of

MASTER OF SCIENCE

June 1966

APPROVED:

[redacted]

Professor of Chemistry

In Charge of Major

[redacted]

Chairman of Department of Chemistry

[redacted]

Dean of Graduate School

Date thesis is presented 11 May 1966

Typed by Gail Dailey

ACKNOWLEDGMENTS

I am indebted to Dr. Harry Freund for guidance throughout the writing of this thesis. Gratitude is expressed to Professor Paul Delahay of New York University for his helpful consultation on adsorption. Dr. R. W. Stromatt provided many helpful suggestions throughout the laboratory phase of this work. Dr. F. P. Roberts and Dr. E. J. Wheelright aided this study by making available a gram of promethium-147, which would have been unobtainable otherwise. Thanks are due to the management and personnel of the Chemical Research and Analytical Chemistry sections of Battelle Northwest for their assistance in this work.

Appreciation is extended to the Inter-University Fellowship Committee for their financial support of this project, and to the Atomic Energy Commission and Battelle Northwest for the use of their facilities at Richland, Washington.

TABLE OF CONTENTS

LIST OF FIGURES

LIST OF TABLES

CHRONOPOTENTIOMETRY OF Sm(III) AND Pm(III) IN MOLTEN LiCl-KCl EUTECTIC

INTRODUCTION

This project originated primarily in support of the Hanford Salt Cycle program (2, 3), a method of reprocessing spent UO_2-PuO_2 nuclear fuel elements. In this process, the declad fuel elements are dissolved in molten LiCl-KCl by sparging with HCl gas and then electrolyzed in the presence of a O_2-Cl_2 sparge to deposit UO_2-PuO_2 solid solutions. These deposits are thus partly separated from the nuclear poisons generated by the fission of the fuel. Since about half of the nuclear poisoning is due to rare earths, it was of interest to investigate the electrochemical behavior of rare earths in molten LiCl-KCl.

Samarium and promethium were chosen because it was also of interest to investigate the possibility of developing a simple method of electrochemical separation to replace the present cumbersome ion exchange methods.

Campbell (7, p. 1) had earlier investigated the chronopotentiometric behavior of samarium in connection with his development of a third-order disproportionation scheme for divalent rare earths. However interpretation of his results for samarium was limited because of alloying with his platinum electrodes.

THEORY

General Theory

Chronopotentiometry involves the passage of a constant current between an indicator electrode and a counter electrode and observation of the potential of the indicator electrode versus a reference electrode. See Figure 1.

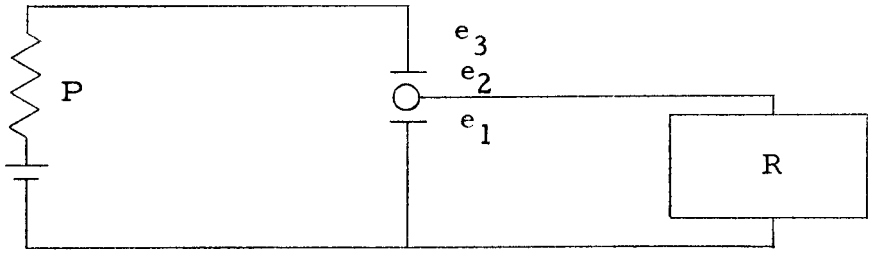

Figure 1. Schematic of chronopotentiometric circuit

P = constant current power supply

R = potential recording device

e_1 = working electrode

e_2 = reference electrode

e_3 = unpolarized counter electrode

Electrolysis at controlled current was used by Weber in 1879 (51) to verify Fick's second law of diffusion. The theory was first developed by Sand and Karaoglanoff in the early 1900's (21, 40) and expanded by Delahay and co-workers in the early 1950's (10, p. 179, 11). Since then, the number of workers in the field has grown rapidly.

In order that rigorous equations may be derived for the potential-time relationships for this system, it is necessary that several conditions be met. They are: linear diffusion must apply, convection and migration must be negligible, and the fraction of the current used in charging the double layer should be negligible.

For a simple reduction where these conditions are met, the relationships between concentration and distance from the electrode have been derived (21, 40, 51):

$$C_O(x,t) = C^0 - \frac{2 D_O^{\frac{1}{2}} t^{\frac{1}{2}}}{\pi^{\frac{1}{2}}} \exp -\frac{x^2}{4D_O t} + \lambda x \operatorname{erfc} \frac{x}{2D_O^{\frac{1}{2}} t^{\frac{1}{2}}} \qquad (1)$$

$$C_R(x,t) = \frac{2\lambda D_O t^{\frac{1}{2}}}{D_R^{\frac{1}{2}} \pi^{\frac{1}{2}}} \exp \frac{-x^2}{4D_R t} - \frac{\lambda x D_O}{D_R} \operatorname{erfc} \frac{x}{2D_R^{\frac{1}{2}} t^{\frac{1}{2}}} \qquad (2)$$

where $\lambda = \frac{I}{nFD_O}$

and,

C^0 = the concentration in the bulk of the solution in moles per cubic centimeter

x = the distance from the electrode surface in centimeters

$C_O(x,t)$ = the concentration of the oxidized form of the depolarizer

$C_R(x,t)$ = the concentration of the reduced form of the depolarizer

D_O = diffusion coefficient of the oxidized form

D_R = diffusion coefficient of the reduced form

t = the time in seconds

I = current density

$$\text{erfc } B = 1 - \text{erf } B = 1 - \frac{2}{\pi^{\frac{1}{2}}} \int_0^B \exp(-Z^2)dZ$$

Equations (1) and (2) may be substituted into the Nernst equation:

$$E = E^0 + \frac{RT}{nF} \ln \frac{f_O D_R^{\frac{1}{2}}}{f_R D_O^{\frac{1}{2}}} + \frac{RT}{nF} \ln \frac{C^0 - Pt^{\frac{1}{2}}}{Pt^{\frac{1}{2}}} \qquad (3)$$

where $P = \dfrac{2I}{\pi^{\frac{1}{2}} nF D_O^{\frac{1}{2}}}$

and,

E = electrode potential in volts

E^0 = the standard formal potential in volts

R = gas constant

T = absolute temperature

n = number of electrons transferred per ion

F = Faraday constant

f = activity coefficient

The first two terms of equation (3) equal the polarographic half-wave potential, $E_{\frac{1}{2}}$. Equation (3) may then be written as

$$E = E_{\frac{1}{2}} + \frac{RT}{nF} \ln \frac{C^0 - Pt^{\frac{1}{2}}}{Pt^{\frac{1}{2}}} \qquad (4)$$

When the concentration, at the surface of the electrode, of the species being reduced reaches zero, there is a rapid change in potential at a time τ which may be defined by:

$$\tau^{\frac{1}{2}} = \frac{C^0}{P} \qquad (5)$$

Equation (5) is then substitued in equation (4) giving:

$$E = E_{\frac{1}{2}} + \frac{RT}{nF} \ln \frac{\tau^{\frac{1}{2}} - t^{\frac{1}{2}}}{t^{\frac{1}{2}}} \qquad (6)$$

From equation (6) it can be shown that the polarographic half-wave potential corresponds to the chronopotentiometric quarter-wave potential, that is, E at $t = \tau/4$.

For a reversible reaction, a plot of the $\log \left(\frac{\tau^{\frac{1}{2}} - t^{\frac{1}{2}}}{t^{\frac{1}{2}}} \right)$ versus E should be a straight line of slope $\frac{nF}{2.3\,RT}$. This allows the determination of n from experimental data.

Substituting for P in equation (5) gives:

$$\tau^{\frac{1}{2}} = \frac{\pi^{\frac{1}{2}} nF C^0 D_O^{\frac{1}{2}}}{2I} \qquad (7)$$

Thus $\tau^{\frac{1}{2}}$ is proportional to C^0 and $1/I$.

According to equation (7), a plot of $I\tau^{\frac{1}{2}}$ versus I should be a straight line of zero slope. This relationship serves as a convenient test of the presence of kinetic or adsorption complications.

Kinetic Complications

If there is a chemical reaction preceding or following the electrochemical reduction, the kinetic rates involved complicate the equations derived for the simple case by affecting the concentration of the substance being reduced.

For example, consider a kinetic system of the following type:

$$Y \underset{k_r}{\overset{k_f}{\rightleftharpoons}} O \xrightarrow{ne} R$$

where,

k_f = forward rate constant

k_r = reverse rate constant

ne = electrochemical reduction

O = oxidized form

R = reduced form

Here, Y is some substance that is transformed into substance O by a chemical reaction. It is assumed that Y is not directly reduced at the potentials involved. The rate of the chemical reaction will affect the concentration of O and thus will also affect the transition time.

The differential equation for the concentration of O has been solved by Delahay and Berzins (11), giving this result:

$$C_O(0,t) = \frac{1}{1+\frac{k_b}{k_f}} \left(C^0 - 2\lambda \left(\frac{Dt}{\pi}\right)^{\frac{1}{2}} - \lambda \frac{k_b}{k_f} \frac{D^{\frac{1}{2}}}{(k_f+k_b)^{\frac{1}{2}}} \operatorname{erf} \left[(k_f+k_b)^{\frac{1}{2}} t^{\frac{1}{2}}\right] \right) \tag{8}$$

D is the common value of D_O and D_R which are assumed to be equal and λ is defined by $\lambda = \frac{I}{nFD_O}$. The transition time is determined by $C_O(0,t) = 0$, and τ_k may be calculated from equation (8). Substituting for λ and rearranging terms gives:

$$I\tau_k^{\frac{1}{2}} = \frac{\pi^{\frac{1}{2}} nFC^0 D^{\frac{1}{2}}}{2} - \frac{\pi^{\frac{1}{2}} I}{2K(k_f+k_b)^{\frac{1}{2}}} \operatorname{erf} \left[(k_f+k_b)^{\frac{1}{2}} \tau_k^{\frac{1}{2}}\right] \tag{9}$$

Experimentally, $K(k_f+k_b)^{\frac{1}{2}}$ may be calculated from the slope, $m = \frac{\pi^{\frac{1}{2}}}{2K(k_f+k_b)^{\frac{1}{2}}}$, of the $I\tau^{\frac{1}{2}}$ versus I plot for cases of kinetic control. If K is known, then k_f and k_b may be calculated.

If typical values of the variables are substituted into equation (8) and a plot of $I\tau^{\frac{1}{2}}$ versus I is made, it can be shown that the resulting plot always has a zero or negative slope (10, p. 203).

Similar solutions have been obtained for a number of other kinetic schemes by other workers (36, 45). All of the solutions give either a zero slope for very large or very small rate constants, or a negative slope for intermediate rate constants.

Adsorption

Adsorption was first studied by means of chronopotentiometry by Lorenz (28). Since his work, other studies have been made by Reinmuth (36). The theory has been developed by both Lorenz and Reinmuth.

The transition time for a surface active species is given by the sum of the terms for the reduction of the active species adsorbed on the electrode and the component that diffuses from the solution:

$$\tau = \tau_a + \tau_d \tag{10}$$

τ = total transition time

τ_a = time necessary to reduce the adsorbed component to zero

τ_d = time necessary to reduce the diffusing species to zero at the electrode surface

τ_a is determined by the electrode area, the amount of adsorbed material per unit area, and the number of electrons involved in the electrochemical reduction.

$$\tau_a = \frac{nF\Gamma}{I} \tag{11}$$

Γ = amount of material adsorbed

τ_d is the conventional transition time given by equation (7). Thus, equation (10) may be rewritten:

$$\tau = \frac{nF\Gamma}{I} + \frac{n^2F^2\pi D_O C^2}{4I^2} \qquad (12)$$

or,

$$I\tau = nF\Gamma + \frac{n^2F^2\pi D_O C^2}{4I} \qquad (13)$$

Thus, a straight line plot of $I\tau$ versus $1/I$ for a given concentration should give an extrapolated intercept of $nF\Gamma$ and have a slope equal to $\frac{n^2F^2\pi D_O C^2}{4}$.

If the electrode surface becomes saturated with respect to the single adsorbing species, the intercept should remain constant even though the concentration of the adsorbed species is increased beyond the saturation concentration. If monolayer adsorption is assumed at the saturation point, the area occupied by a single molecule may be calculated:

$$\text{molecular area} = \frac{A}{N\Gamma}$$

where,

A = electrode area

Γ = amount adsorbed

N = Avogadro's number

The contributions of adsorption to the transition time increases and that of diffusion decreases as the current density increases. This has several results: a plot of $I\tau$ versus I has a positive slope, a plot of $\tau^{\frac{1}{2}}$ versus C (at constant I) has a negative intersection

with the abscissa rather than zero or a positive one, and the temperature coefficient of τ tends to be negative rather than positive.

APPARATUS

Salt Filtration Apparatus

The glassware used in the filtration is shown in Figure 2. All "item" numbers refer to that figure.

The cell, item 5, was a Vycor[1] tube, 64 mm in diameter and 275 mm long with a 6 mm ground flange on the top.

The cell top, item 6, was a cap made of Pyrex[1] glass 64 mm in diameter and about 30 mm high, also with a 6 mm ground flange. There was a 12/5 ball joint on the side, two 19/38 female standard taper joints, one 10/30 female standard taper joint, and an 8 mm outside diameter tube on the top.

The special cell top, item 7, was made of a disc of 1/8 inch thick quartz, 64 mm in diameter with a 20 mm diameter hole in it.

The isolated compartment, item 1, was made of 12 mm outside diameter quartz tubing, with a 10 mm coarse frit inside the lower end and a 19/39 male standard taper on the other end.

The filter tube, item 8, was a Pyrex tube of 10 mm inside diameter with a 20 mm medium Pyrex frit on one end and a male 18/9 ball joint on the other. It was of sufficient length to reach the bottom of the cell and it allowed the collecting tube to be connected at a distance of about eleven inches from the cell.

---

[1]Registered trademark: Corning Glass Company, Corning, New York.

The collecting tube, item 3, consisted of three 30 mm Pyrex tubes joined together at top and bottom with 10 mm outside diameter Pyrex tubing. Two of the tubes had female 18/9 socket joints on them. This arrangement allowed the filtered salt to be conveniently divided into three equal portions.

The reference electrodes, item 10, were made of 6 mm outside diameter Pyrex tubing, 350 mm long with a male 10/30 standard taper joint on the upper end. The lower ends were melted shut and blown into test-tube ends and were carefully annealed. They were filled with sufficient 0.1 molal AgCl in LiCl-KCl eutectic salt to fill the tubes about 40 mm. A clean silver wire of sufficient length to reach out of the tube was then dipped into the salt. The top of the tube was then closed with a small cork.

The tungsten electrode, item 2, was made by spot-welding a 24.4 cm^2 tungsten sheet 7 mils thick to a 20 gauge tungsten wire that was 16 inches long. The tungsten electrode was cleaned between each run by dipping it into aqua regia. The tungsten wire above the melt was protected by a sheath of 2 mm quartz tubing that reached out of the top of the cell.

The isolated electrode was a 1/8-inch diameter graphite[2] rod 12 inches long which was lengthened by threading the end and

---

[2] Spectrographic graphite produced by the National Carbon Company, New York, New York

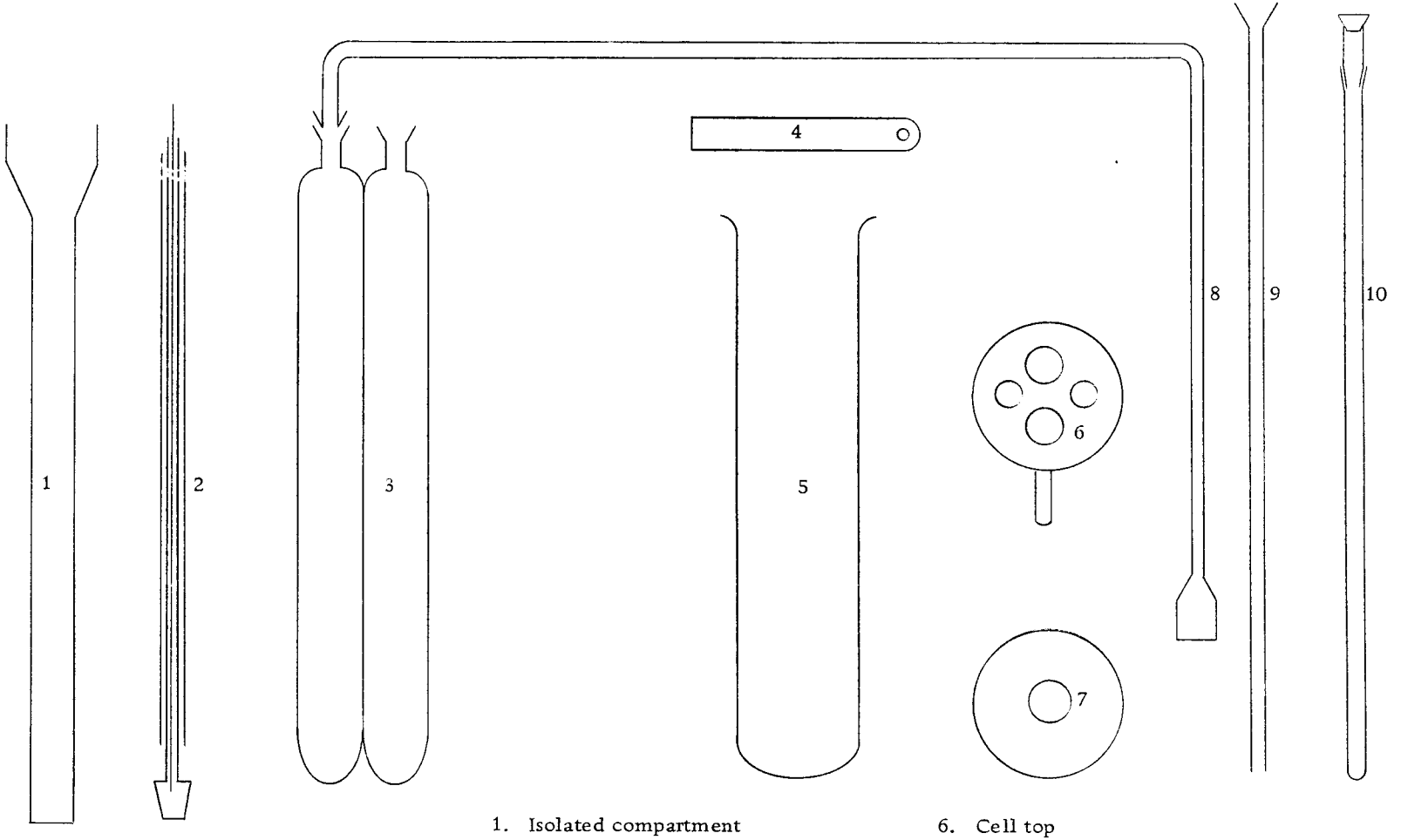

Figure 2. Salt Filtration Apparatus

1. Isolated compartment
2. Tungsten electrode
3. Collecting tube
4. Six-inch ruler
5. Cell
6. Cell top
7. Special cell top
8. Filter tube
9. Sparge tube
10. Reference electrode

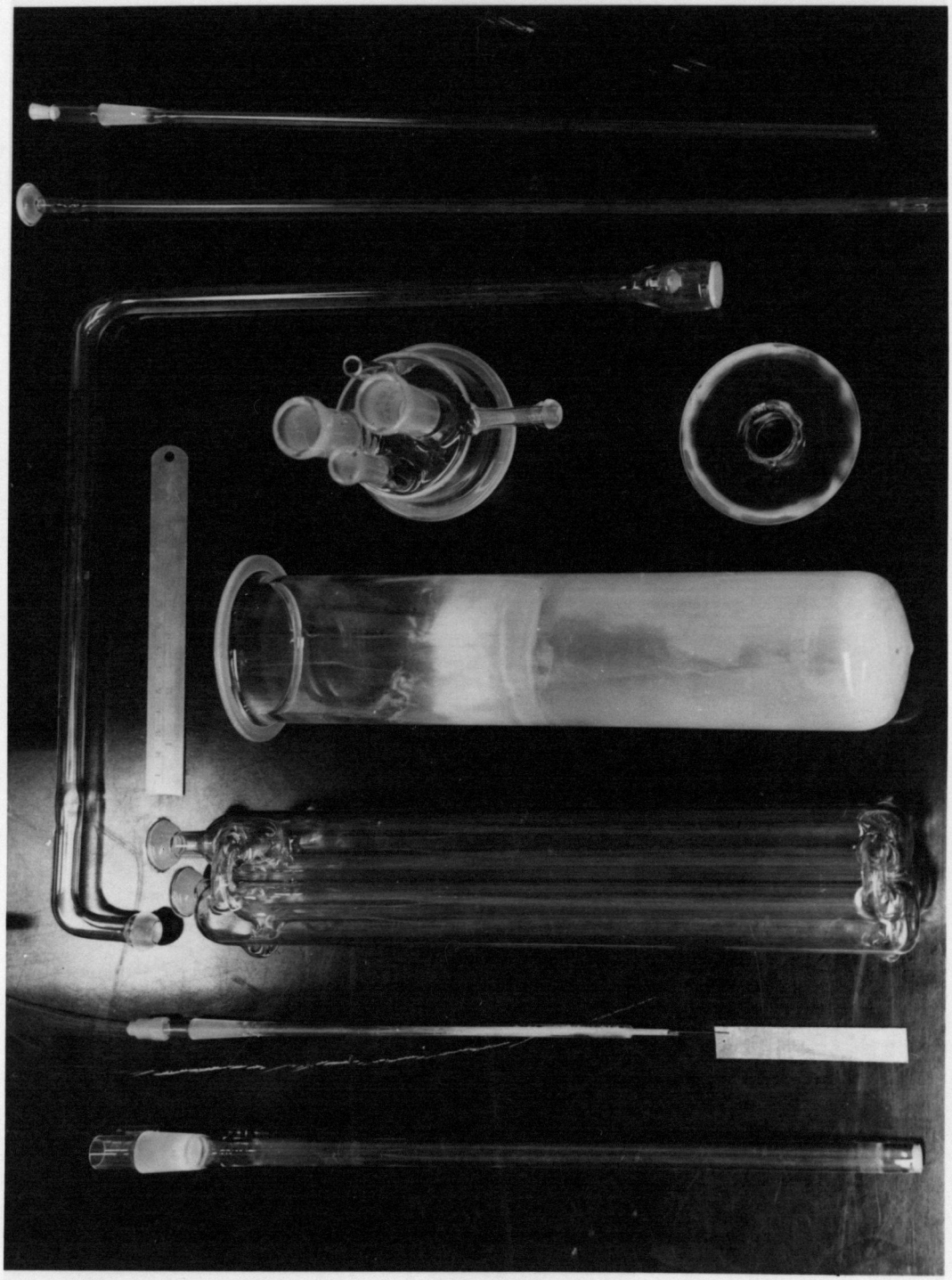

screwing it into a threaded hole in another graphite rod which had a $\frac{1}{4}$-inch diameter and was 4 inches long. This additional length was necessary to allow electrical connection to be made to the electrode.

The furnaces, which consisted of 1200 watt heating elements with magnesia liners, were constructed at Hanford. The center holes of these furnaces had a diameter of 3 inches and were 10 inches deep.

During the pre-filtration electrolysis, the potential of the tungsten electrode was controlled by an Electronisher Potentiostat nach Werding which is manufactured by the Gerhard Bank Elektronic of Göttingen, Germany.

Gas Purification

The cylinder argon was analyzed with a mass spectrometer and found to contain 300 parts per million oxygen. The argon used for the melt filtration was purified by passing it over powdered titanium at 900°C. The titanium was contained in a 30 mm by 600 mm quartz tube which was placed in a tube furnace. The argon was then passed through a $Mg(ClO_4)_2$ drying column. This treatment reduced the oxygen content to less than 100 parts per million, which was the detection limit for the mass spectrometer used. However, the TiO_2 formed sinters at the temperature used, making it difficult to clean the tube so that it may be recharged with fresh titanium.

For this reason, it was decided to use helium for the chronopotentiometer cell since cylinder helium generally has a low oxygen content. This was confirmed by mass spectrometer analysis which showed the oxygen content of the helium to be about 400 ppm. The helium was first passed through a $Mg(ClO_4)_2$ drying column. The oxygen was then removed by flowing the helium through a 10 mm by 250 mm Vycor tube filled with pieces of zirconium metal at a temperature of about 900°. An analysis of the gas showed the oxygen content to be less than 100 ppm. Next, it passed through a trap filled with glass wool and a fine glass frit to remove any entrained dust particles.

The downstream side of both cells was protected with a $Mg(ClO_4)_2$ drying column and a H_2SO_4 trap to prevent moisture from backing up the gas line.

The HCl was dried before use by passing it through two $Mg(ClO_4)_2$ drying columns.

Chronopotentiometer and Associated Apparatus

The chronopotentiometer required a constant current source which was obtained by dropping 300 volts from a power supply across the resistance necessary to give the current desired. A selector

switch was provided which allowed the proper resistance to be switched into the circuit to give a current range of 0.44 to 40 milliamperes. The IR drop of 1 or 2 volts across the cell is negligibly small when compared to the total IR drop of 300 volts. The current was determined by measuring the IR drop across a precision resistor with a Hewlett-Packard 3440A Digital Voltmeter.

The reference electrodes and isolated electrode were the same as the ones used for the melt filtrations.

Platinum working electrodes were constructed by forming a bead, approximately 1 mm in diameter, by melting the tip of the wire with an oxy-propane torch. The wire was then sealed into Pyrex tubing. Tungsten working electrodes were made by spot-welding 1 cm^2 tungsten sheets of 5 mil thickness to the end of a piece of 0.5 mm diameter tungsten wire about 16 inches long. Before it was welded, the tungsten sheet was polished to a near-optical finish by conventional polishing techniques. These electrodes were difficult to make since the spot-welding was done in air. However, good welds could be made after the proper current and duration were determined by trial-and-error. Any tungsten oxide formed during the welding was removed by hydrogen-reducing the electrode at 850^{o} overnight. The resulting electodes were of a bright, metallic luster. The area was calculated by measuring the dimensions of the

electrode with a caliper rule. A sheath of 2 mm quartz tubing was used to protect the tungsten wire above the melt. The furnace used was the same as the ones used for the salt filtration.

The temperature was controlled with a Honeywell-Brown Pyr-O-Vane Controller.

The potential changes observed in the chronopotentiometric measurements were determined with a Honeywell 906C Visicorder which utilized a beam of light focused on light-sensitive paper.

Temperatures were read by measuring the potential of a Chromel-Alumel thermocouple with a Gray Instrument Company Model E-3048DT potentiometer.

PROCEDURE

Melt Filtration

The melt used in these experiments was the LiCl-KCl eutectic. The salts as supplied by the manufacturer contain appreciable amounts of metals such as nickel, manganese, and iron (38, p. 1). Therefore the salts must be purified before use. This purification was achieved by a pre-electrolysis of the eutectic mixture. Since the metal deposit did not adhere to the electrode, it was necessary to filter the melt.

The salts were dried in a vacuum oven at 110° for several weeks before they were used. Since the collecting tube could be conveniently designed to hold enough salt for three different chronopotentiometric runs, the filtration was performed on 600 g batches of salt. Therefore, 327 g of KCl and 273 g of LiCl were weighed, as quickly as possible to minimize water pickup from the air, directly into the Vycor cell. The cell top was then put on and fastened in place with battery clips and dry HCl was passed through the cell which was kept at room temperature for a half hour. The cell was then placed in a furnace and the temperature increased to 300° for two hours (24). The temperature was then increased to 500° and the melt sparged with dry HCl gas overnight. The next morning, the HCl was turned off and the melt was sparged with Cl_2-O_2 to remove

any carbon present in the melt. After two hours, the Cl_2-O_2 sparge was turned off, and the melt was again sparged with HCl for two hours to remove the oxides present. The HCl sparge was then turned off and the HCl present in the cell was removed by sparging with dry argon for a half hour.

The reference electrode, isolated electrode, and isolated compartment were then dried in a tube furnace and placed in the cell. The tungsten electrode was lowered into the cell in four stages of about a minute each so that it would be dry when it was placed in the melt. Next, a constant potential electrolysis was carried out. It was found that the deposit adhered to the electrode better if the electrolysis was begun at 1.500 volts and increased to 1.900 volts in steps of 0.100 volts of about one hour duration. The electrolysis was continued overnight. Currents ranged from about 100 milliamps initially to about 5 milliamps at the end of the electrolysis.

After the electrolysis was completed, the electrodes were removed from the cell and the cell top removed. The filter tube was then inserted into the cell and the special cell top clamped on. Dry argon was passed through the cell above the melt. The collecting tube was then placed in a furnace and connected to the filter tube. A vacuum pump was connected to the other 18/9 socket, and a vacuum applied. The melt was thus pulled through a medium Pyrex frit into the collecting tube. The salt was kept molten in the filter tube by

carefully warming the tube with cool flames from two hand-held oxygen-propane glass-blowing torches. The salt was also kept molten in the collecting tube so that the tube would fill evenly.

After the salt was filtered, the filter tube and vacuum pump were disconnected from the collecting tube and the 18/9 socket joints were closed by 18/9 ball joints that had been sealed at one end. The collecting tube was then cooled rapidly by blowing cool air on it with a hand-held air gun. This air gun had a heating element, a small fan, and a three-way switch which allowed the gun to produce a stream of air at either 1000°F or room temperature, depending on whether the heating element was included in the circuit. When the salt was frozen, it was placed in a vacuum oven until needed.

Chronopotentiometry

The filtered salt was transferred into the drybox as needed and the glass was broken off the salt with a pestle. About 175 g of salt was weighed directly into the chronopotentiometer cell and melted using the same procedure as for the salt filtration. After the melt had been sparged overnight with HCl, a blank was run using the procedure below. The desired quantity of rare earth oxide was weighed into a sample boat, which was a quartz test tube 10 mm in diameter and 10 mm long. The sample boat was dropped into the melt and the cell was shaken by hand, spilling most of the oxide into the melt.

The oxide was dissolved by sparging overnight with HCl.

After a half hour helium sparge, the electrodes and isolated compartment were lowered into the cell in four or five steps of about a minute each, both to make sure they were dry and to avoid breaking the reference electrode. The electrodes were then connected to the chronopotentiometer leads.

Chronopotentiograms were run at some convenient current density until a constant transition time was reached. This usually took about an hour. Chronopotentiograms were then run over a range of transition times of about 30 milliseconds to two seconds, or the observable limits, for each concentration. About 5-8 different current densities were measured at each concentration. For several different concentrations, chronopotentiograms were run at three different temperatures about 100° apart. For a few runs, the current was reversed just after the transition time to study the reversibility of the reaction. Most of the runs, however, were reductions only.

For these, the rare earth thus deposited was oxidized off and the cell was let equilibrate for at least four minutes before another run was made.

After each run was finished, the electrodes were removed from the cell, the argon was turned off, and the next addition of rare earth oxide was made. The temperature controller was adjusted to 500°C, and the cell was sparged overnight with HCl. Any unused standard

taper joints in the cell top were blanked off with male standard taper joints that had been sealed shut at one end.

During the chronopotentiometric runs, the temperature was measured with a Chromel-Alumel thermocouple, sheathed with 2 mm quartz tubing, placed in the isolated compartment. At all other times the temperature was measured with a Chromel-Alumel thermocouple positioned in the furnace next to the cell.

Promethium

The promethium was obtained as 350 mls of 2.8 g/l solution of promethium-147 in 0.2 M HNO_3. It was precipitated at 55 °by the addition of 100 mls of 1M oxalic acid. The precipitate was filtered through a Pyrex frit and dried overnight. The pink oxalate thus obtained was then transferred to a 25 mm by 200 mm tube and calcined at 700 °C. The oxide was transferred to the drybox and added to the melt in weighed amounts.

This oxide proved to be very difficult to dissolve. The dissolution was finally accomplished by sparging the melt overnight with Cl_2 at 650 ° in the presence of a $\frac{1}{4}$-inch carbon rod.

RESULTS AND DISCUSSION

The data were obtained in the form of chronopotentiograms, see Figures 3 and 4. The runs were made at known temperatures, current densities, and concentrations. Transition times were calculated by the method of Reinmuth, see Figure 3. Lines ABC and DEF and an intersecting line BE were drawn and the transition time was taken as the time between E and G on a line parallel to the t axis. In theory, the line AB should be parallel to E, the voltage axis, but in practice this is not the case. Charging of the double layer causes this segment to have a small slope. If the electrode surface is extremely rough, or if it has an oxide coating, the charging current will be large and the chronopotentiogram will be difficult or impossible to interpret. The high slope of the BE portion is due to the depletion of the ions near the electrode surface. At the point E, the transition time, the surface concentration of reactive ions is zero and the process becomes diffusion controlled, resulting in a decrease in slope. Eventually, about point F, the slope increases again as the solvent decomposes. The currents used were determined by measuring the IR drop across a precision resistor with a digital voltmeter. The electrode area was then measured with a caliper rule and the current density calculated.

Van Artsdalen and Yaffe (49) have measured the density of

several melts as a function of melt composition and temperature. The density of the LiCl-KCl eutectic as a function of temperature was interpolated from their data. Since the total weight of the eutectic and the weight of samarium oxide added were known, it was possible to calculate the concentration of the samarium. It was assumed that 100 percent of the Sm_2O_3 dissolved. This should be a valid assumption since the promethium was shown by analysis to be nearly all dissolved and it was much more difficult to dissolve since the Pm_2O_3 had been sintered unintentionally.

The promethium concentration was determined by radiochemical analysis. After the chronopotentiometric run was finished, a 0.8 gram sample of the melt was taken and transferred to a wetbox. Here, the light-violet colored sample was dissolved in 10 mls of 1.5M HCl and a 1 ml sample sent to the counting laboratory.[3] An aliquot of this sample was taken and a total-beta count made. The concentration of promethium in the original sample was then calculated from the measured activity and the half-life of Pm^{147}.

The first plots of the data were of $I\tau^{\frac{1}{2}}$ versus I. All of the graphs had a positive slope, indicating adsorption of the electroactive species. A specific test for adsorption (36) was made by plotting $\tau^{\frac{1}{2}}$ versus concentration at constant I. The intersection with the abscissa was negative, confirming the presence of adsorption.

[3] The promethium activity in this sample was 8.2×10^{10} d/m/ml.

Adsorption has not previously been observed for other rare earth ions (7, p. 1) or for similar ions (24, 31) in the molten LiCl-KCl eutectic.

If adsorption occurs, the diffusion coefficient may be calculated from the slope:

$$m = I^2\tau = \frac{n^2F^2\pi D_O C^2}{4}$$

of a plot of $I\tau$ versus $1/I$ (8, p. 11).

The values calculated in this manner for samarium are shown in Table 1.

Table 1. D_O Values for Sm(III), 484°

Run	Temperature (°C)	Concentration (moles/cm^3)	D_O(cm^2/sec)
Sm 12	484	2.02×10^{-6}	2.3×10^{-6}
Sm 13	484	3.97×10^{-6}	2.04×10^{-6}
Sm 15	484	7.30×10^{-6}	2.84×10^{-6}
Sm 16	482	1.24×10^{-5}	2.82×10^{-6}

Diffusion coefficients for Sm(III) were also calculated for other temperatures as shown in Table 2.

Table 2. D_O Values for Sm(III), Various Temperatures

Run	Temperature	Concentration (moles/cm^3)	D_O (cm^2/sec)
Sm 12	395°	2.07×10^{-6}	1.33×10^{-6}
Sm 14	376°	5.72×10^{-6}	0.94×10^{-6}
Sm 14	573°	5.34×10^{-6}	5.14×10^{-6}
Sm 16	385°	1.28×10^{-5}	1.30×10^{-6}
Sm 16	577°	1.21×10^{-5}	4.59×10^{-6}

These values compare favorably with the values obtained for similar ions in the same melt which are listed in Table 3.

Table 3. D_O Values for Several Ions

Ion	D_O (cm^2/sec)	Reference	Temperature
Bi(III)	6×10^{-6}	24	450°
Cd(II)	1.7×10^{-5}	24	450°
Ag(I)	2.6×10^{-5}	24	450°
Cu(I)	3.5×10^{-5}	24	450°
Pu(III)	5.1×10^{-6}	31	400°
Eu(III)	6.1×10^{-6}	7, p. 64	450°
Yb(III)	2.2×10^{-6}	7, p. 64	450°

The diffusion coefficient for Sm(III) was also calculated by extrapolating the $I\tau^{\frac{1}{2}}$ versus I plots to zero current density (Figure 5) and plotting the $I\tau^{\frac{1}{2}}$ values thus obtained versus concentration (Figure 9). The slope of this plot is $m = \frac{I\tau^{\frac{1}{2}}}{C}$. The diffusion coefficient was calculated by means of the relationship:

$$I\tau^{\frac{1}{2}} = \frac{\pi^{\frac{1}{2}} nFCD_O^{\frac{1}{2}}}{2}$$

to be 3.1×10^{-6} cm^2/sec which is in fair agreement with the value obtained earlier.

Due to experimental difficulties, only a limited amount of data were available for promethium. D_O for Pm(III) at 488° was calculated from the zero intercept of the $I\tau^{\frac{1}{2}}$ versus I plot as 2.3×10^{-6} cm^2/sec, which is in good agreement with the values obtained for samarium.

Several sources of error exist in the determination of D_O. Probably the largest was the error involved in drawing lines BE and EF. See Figure 3. The segment EF often had a slight curvature due to the double layer charging current. Also, the width of the lines was important on the small scale involved. Even though a 10 X hand lens was used to check the placement of the lines, it was estimated that errors up to 10 percent of the transition time would occur on chronopotentiograms made at low concentrations or near the observable limits of the current densities used. At higher

concentrations and at intermediate current densities, this error decreased to less than 1 percent. No data were used unless the transition time was reproducible to 5 percent or better If all of the transition times are determined at the same potential and in the same manner, a systematic error is introduced such that a given transition time may be reproducible to ± 5 percent and still involve a ± 10 percent uncertainty. If the transition times are not measured in a consistent manner, the points at a given current density will tend to scatter, resulting in a reproducibility of about 10 percent for borderline points. For the most favorable concentrations and current densities used here, the total errors for a given point decreased to about ± 2 percent, e.g. points determined at intermediate current densities for Sm 15 at 484°. Other sources of error, although they were small, were the evaporation of LiCl at the higher temperatures used and the splattering of salt during sparging. These were minimized by running at high temperatures for as short a time as possible and by sparging at moderate flow rates, about 150 ml/min in all cases. Also, the lower portion of the tube was rinsed with the molten eutectic on occasion so that any globules of salt frozen on the cell would be remelted. During the promethium runs it was possible to check for possible volitilization of the rare earth chloride by surveying the cell with a Hanford CP-TP high-level

beta-gamma detector. As expected, the promethium was found to be confined to the melt.

The limited amount of data for promethium make it difficult to determine the experimental error exactly. However, since the calculations for promethium are very similar to the ones for samarium, the error is probably about ± 15 percent.

For reversible reactions, the transition time for the oxidation process is one third the time for the reduction process (10, p. 195). Experimentally, both these values may be conveniently determined by reversing the current just after the reduction wave for the substance being studied. If the reaction is reversible, it is possible to calculate n from the slope of a plot of $\log \frac{\tau^{\frac{1}{2}} - t^{\frac{1}{2}}}{\tau^{\frac{1}{2}}}$ versus E. The slope is $\frac{nF}{2.3RT}$.

However, for Sm(III) and Pm(III) the transition time ratios were 0.46 and 0.51 respectively, indicating that the reactions were irreversible. Thus, it was not possible to calculate n directly. A value of 3 was assumed in the calculations.

The quarter-wave potentials were determined for Sm(III) and Pm(III) by measuring the potential at $t = \tau/4$. The quarter-wave potential for Sm(III) decreased steadily as the current density increased. However, when the values were averaged, they were constant to ± 5 percent. The value for Pm(III) was more constant as the current density increased, but was slightly erratic. However,

it was also constant to ± 5 percent. The quarter-wave potentials were: Sm(III), -0.95 ± 0.05 volts; and Pm(III), -1.21 ± 0.06 volts versus Ag-AgCl. Campbell (7, p. 112) measured the samarium potential as -1.74 volts, europium as -0.51 volts, and ytterbium as -1.35 volts versus Pt-Pt(II). Ag(I) is about -0.3 volts with respect to Pt-Pt(II).

It was not possible to determine the adsorption isotherm since the saturated value for Γ was not observed.

Chronopotentiometry was found to be a relatively convenient method of investigating molten salt systems. The most serious experimental difficulties encountered were gas purification systems and preparation of the tungsten electrodes. It was also possible to work safely with highly radioactive materials under these conditions. After calcination, the gram of promethium-147 was reading approximately 80 R at a distance of about 1 inch.

It should also be feasible to separate small amounts of samarium from large amounts of promethium (a situation that arises in isotopic power supplies) since the quarter-wave potentials differ by 0.26 volts.

Table 4. Quarter-Wave Potentials for Sm(III) and Pm(III)

Sm		Pm	
$I \times 10^3$ (amp/cm^2)	$E_{\frac{1}{4}}$ (volts)	$I \times 10^3$ (amp/cm^2)	$E_{\frac{1}{4}}$ (volts)
3.07	0.98	3.00	1.13
4.36	0.973	4.27	1.18
5.35	0.957	4.60	1.24
6.55	0.948	5.23	1.18
10.7	0.935	6.43	1.36
12.5	0.935	10.5	1.22
16.7	0.945	12.2	1.19
22.5	0.905		
Average	0.95 ± 0.05	Average	1.21 ± 0.06

Table 5. Data, Sm 12, 484°

$C = 2.02 \times 10^{-6}$ moles/cm^3					
$I \times 10^3$ (amp/cm^2)	τ sec	$I\tau \times 10^3$ ($\frac{\text{amp-sec}}{\text{cm}^2}$)	$1/I \times 10^{-2}$ cm^2/amp	$\tau^{\frac{1}{2}}$ sec$^{\frac{1}{2}}$	$I\tau^{\frac{1}{2}} \times 10^3$ ($\frac{\text{amp-sec}}{\text{cm}^2}$)
0.99	1.02	1.01	10.1	1.01	1.00
2.09	0.310	0.648	4.79	0.557	1.16
3.02	0.134	0.404	3.31	0.366	1.10
4.35	0.0977	0.425	2.30	0.314	1.36
5.33	0.0641	0.341	1.88	0.253	1.35
7.55	0.0377	0.284	1.33	0.194	1.46
10.6	0.0334	0.354	0.943	0.183	1.94

Table 6. Data, Sm 13, 484°

$C = 3.97 \times 10^{-6}$ moles/cm^3					
$I \times 10^3$ (amp/cm^2)	τ sec	$I\tau \times 10^3$ ($\frac{\text{amp-sec}}{\text{cm}^2}$)	$1/I \times 10^{-2}$ (cm^2/amp)	$\tau^{\frac{1}{2}}$ sec$^{\frac{1}{2}}$	$I\tau^{\frac{1}{2}} \times 10^3$ ($\frac{\text{amp-sec}}{\text{cm}^2}$)
0.99	2.41	2.38	10.1	1.55	1.53
2.09	0.641	1.34	4.78	0.800	1.67
3.02	0.355	1.07	3.31	0.595	1.79
4.35	0.200	0.870	2.30	0.447	1.94
5.33	0.135	0.720	1.88	0.367	1.96
6.53	0.104	0.680	1.53	0.322	2.10
7.56	0.0790	0.596	1.33	0.281	2.12
10.7	0.0443	0.474	0.935	0.210	2.25

Table 7. Data, Sm 14, 453°

$C = 5.56 \times 10^{-6}$ moles/cm^3					
$I \times 10^3$ (amp/cm^2)	τ sec	$I\tau \times 10^3$ ($\frac{\text{amp-sec}}{\text{cm}^2}$)	$1/I \times 10^{-2}$ (cm^2/amp)	$\tau^{\frac{1}{2}}$ sec$^{\frac{1}{2}}$	$I\tau^{\frac{1}{2}} \times 10^3$ ($\frac{\text{amp-sec}^{\frac{1}{2}}}{\text{cm}^2}$)
1.04	3.23	3.36	9.62	1.80	1.87
2.10	0.900	1.89	4.76	0.95	1.99
3.07	0.454	1.39	3.26	0.673	2.06
4.36	0.281	1.22	2.30	0.530	2.31
5.35	0.190	1.02	1.87	0.436	2.33
6.55	0.144	0.944	1.53	0.380	2.49
7.60	0.131	0.995	1.32	0.362	2.75
10.7	0.080	0.856	0.935	0.283	2.94

Table 8. Data, Sm 15, 484°

$C = 7.30 \times 10^{-6}$ moles/cm^3					
$I \times 10^3$ (amp/cm^2)	τ sec	$I\tau \times 10^3$ ($\frac{\text{amp-sec}}{\text{cm}^2}$)	$1/I \times 10^{-2}$ (cm^2/amp)	$\tau^{\frac{1}{2}}$ sec$^{\frac{1}{2}}$	$I\tau^{\frac{1}{2}} \times 10^3$ ($\frac{\text{amp-sec}}{\text{cm}^2}$)
2.10	2.63	5.53	4.76	1.62	3.41
3.07	1.22	3.74	3.26	1.10	3.39
4.36	0.660	2.88	2.30	0.812	3.54
4.70	0.565	2.66	2.13	0.750	3.53
5.35	0.445	2.38	1.87	0.666	3.57
6.55	0.324	2.12	1.53	0.569	3.72
7.60	0.248	1.89	1.32	0.498	3.80
10.7	0.133	1.42	0.935	0.355	3.91
12.5	0.101	1.26	0.80	0.318	3.98
16.7	0.0674	1.12	0.60	0.260	4.35

Table 9. Data, Sm 16, 482°

$C = 1.24 \times 10^{-5}$ moles/cm^3					
$I \times 10^3$ (amp/cm^2)	τ sec	$I\tau \times 10^3$ ($\frac{\text{amp-sec}}{\text{cm}^2}$)	$1/I \times 10^{-2}$ (cm^2/amp)	$\tau^{\frac{1}{2}}$ sec$^{\frac{1}{2}}$	$I\tau^{\frac{1}{2}} \times 10^3$ ($\frac{\text{amp-sec}^{\frac{1}{2}}}{\text{cm}^2}$)
3.07	3.28	10.0	3.26	1.81	5.56
4.36	1.70	7.42	2.30	1.30	5.67
5.35	1.10	5.90	1.87	1.05	5.73
6.55	0.766	5.00	1.53	0.875	5.73
10.7	0.298	3.19	0.935	0.545	5.84
12.5	0.251	3.14	0.800	0.500	6.25
16.7	0.153	2.56	0.600	0.391	6.54
22.5	0.083	1.86	0.445	0.299	6.53

Table 10. Data, Sm 12, 395°

$C = 2.07 \times 10^{-6}$ moles/cm^3					
$I \times 10^3$ (amp/cm^2)	τ sec	$I\tau \times 10^3$ ($\frac{\text{amp-sec}}{\text{cm}^2}$)	$1/I \times 10^{-2}$ (cm^2/amp)	$\tau^{\frac{1}{2}}$ sec$^{\frac{1}{2}}$	$I\tau^{\frac{1}{2}} \times 10^3$ ($\frac{\text{amp-sec}^{\frac{1}{2}}}{\text{cm}^2}$)
0.48	2.32	1.11	20.8	1.52	0.730
0.84	1.04	0.874	11.9	1.02	0.857
0.99	0.713	0.706	10.1	0.844	0.835
2.09	0.236	0.495	4.78	0.486	1.02
3.02	0.142	0.429	3.31	0.377	1.14
4.00	0.127	0.508	2.50	0.356	1.42
4.35	0.132	0.575	2.30	0.363	1.58
5.33	0.050	0.267	1.88	0.224	1.19

Table 11. Data, Sm 14, 376

$C = 5.72 \times 10^{-6}$ moles/cm^3					
$I \times 10^3$ (amp/cm^2)	τ sec	$I\tau \times 10^3$ $(\frac{\text{amp-sec}}{\text{cm}^2})$	$1/I \times 10^{-2}$ (cm^2/amp)	$\tau^{\frac{1}{2}}$ sec$^{\frac{1}{2}}$	$I\tau^{\frac{1}{2}} \times 10^3$ $(\frac{\text{amp-sec}^{\frac{1}{2}}}{\text{cm}^2})$
1.04	2.22	2.31	9.63	1.49	1.55
2.10	0.708	1.49	4.76	0.841	1.77
3.07	0.387	1.19	3.26	0.623	1.91
4.36	0.232	1.01	2.29	0.482	2.10
4.70	0.206	0.970	2.13	0.454	2.13
5.35	0.172	0.920	1.87	0.415	2.22
6.55	0.123	0.806	1.53	0.351	2.30
7.60	0.109	0.828	1.32	0.330	2.50
10.7	0.073	0.781	0.935	0.270	2.89

Table 12. Data, Sm 14, 573

$C = 5.34 \times 10^{-6}$ moles/cm^3					
$I \times 10^3$ (amp/cm^2)	τ sec	$I\tau \times 10^3$ $(\frac{\text{amp-sec}}{\text{cm}^2})$	$1/I \times 10^{-2}$ (cm^2/amp)	$\tau^{\frac{1}{2}}$ sec$^{\frac{1}{2}}$	$I\tau^{\frac{1}{2}} \times 10^3$ $(\frac{\text{amp-sec}^{\frac{1}{2}}}{\text{cm}^2})$
2.10	2.26	4.75	4.76	1.50	3.16
3.07	1.08	3.32	3.26	1.04	3.19
4.36	0.558	2.44	2.29	0.746	3.25
5.35	0.373	2.00	1.87	0.610	3.27
6.55	0.250	1.64	1.53	0.500	3.28
7.60	0.190	1.44	1.32	0.436	3.32
10.7	0.100	1.07	0.935	0.316	3.38

Table 13. Data, Sm 16, 385°

$C = 1.28 \times 10^{-5}$ moles/cm^3					
$I \times 10^3$ (amp/cm^2)	τ sec	$I\tau \times 10^3$ $(\frac{\text{amp-sec}}{\text{cm}^2})$	$1/I \times 10^{-2}$ (cm^2/amp)	$\tau^{\frac{1}{2}}$ sec$^{\frac{1}{2}}$	$I\tau^{\frac{1}{2}} \times 10^3$ $(\frac{\text{amp-sec}^{\frac{1}{2}}}{\text{cm}^2})$
3.07	1.75	5.41	3.26	1.20	3.68
4.36	0.956	4.17	2.29	0.977	4.26
5.35	0.644	3.44	1.87	0.803	4.30
6.55	0.465	3.05	1.53	0.682	4.46
7.60	0.386	2.93	1.32	0.662	4.72
10.7	0.214	2.29	0.935	0.463	4.94
12.5	0.175	2.19	0.800	0.418	5.24
16.7	0.123	2.06	0.600	0.351	5.86
22.5	0.0965	2.17	0.445	0.310	6.98

Table 14. Data, Sm 16, 577°

$C = 1.21 \times 10^{-5}$ moles/cm^3					
$I \times 10^3$ (amp/cm^2)	τ sec	$I\tau \times 10^3$ $(\frac{\text{amp-sec}}{\text{cm}^2})$	$1/I \times 10^{-2}$ (cm^2/amp)	$\tau^{\frac{1}{2}}$ sec$^{\frac{1}{2}}$	$I\tau^{\frac{1}{2}} \times 10^3$ $(\frac{\text{amp-sec}^{\frac{1}{2}}}{\text{cm}^2})$
4.36	2.55	11.1	2.29	1.59	6.94
5.35	1.65	8.84	1.87	1.28	6.87
6.55	1.09	7.15	1.53	1.02	6.68
7.60	0.815	6.19	1.32	0.904	6.86
10.7	0.418	4.48	0.935	0.647	6.88
12.5	0.314	3.93	0.800	0.560	7.00
16.7	0.203	3.39	0.600	0.450	7.52
22.5	0.117	2.63	0.445	0.342	7.70
26.0	0.0912	2.37	0.385	0.302	7.85

Table 15. Data, Pm 4, 488°

$C = 7.77 \times 10^{-6}$ moles/cm^3					
$I \times 10^3$ (amp/cm^2)	τ sec	$I\tau \times 10^3$ $(\frac{\text{amp-sec}}{\text{cm}^2})$	$1/I^2 \times 10^{-2}$ (cm^2/amp)	$\tau^{\frac{1}{2}}$ sec$^{\frac{1}{2}}$	$I\tau^{\frac{1}{2}} \times 10^3$ $(\frac{\text{amp-sec}^{\frac{1}{2}}}{\text{cm}^2})$
3.00	1.86	5.58	3.33	1.36	4.08
4.27	1.26	5.38	2.35	1.12	4.77
4.60	1.20	5.52	2.18	1.09	5.02
5.23	1.04	5.45	1.91	1.02	5.33
6.43	0.851	5.47	1.56	0.923	5.95
7.44	0.772	5.74	1.34	0.880	6.55
10.5	0.554	5.82	0.95	0.745	7.82
12.2	0.450	5.50	0.82	0.671	8.18

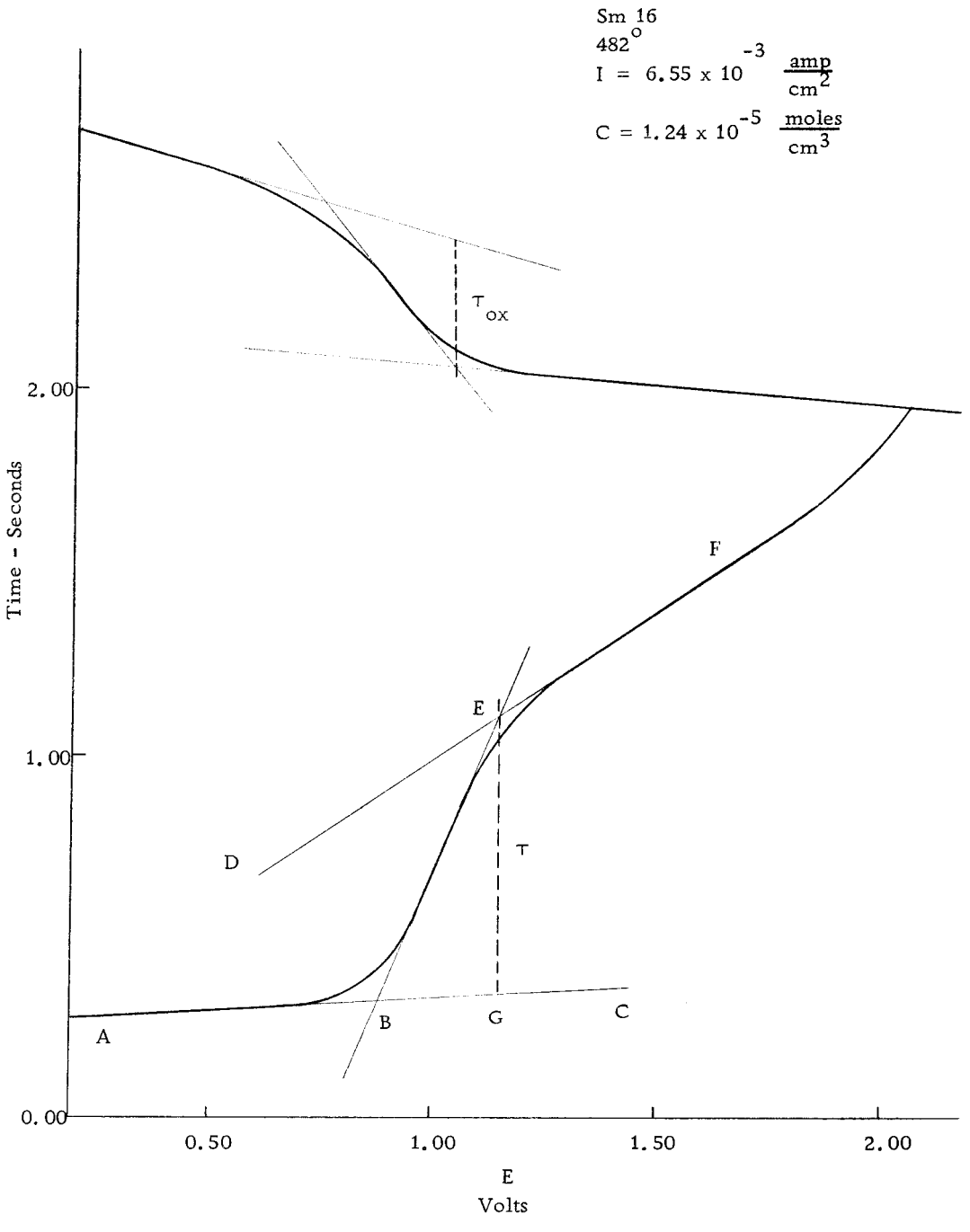

Figure 3. Chronopotentiogram of Sm(III)

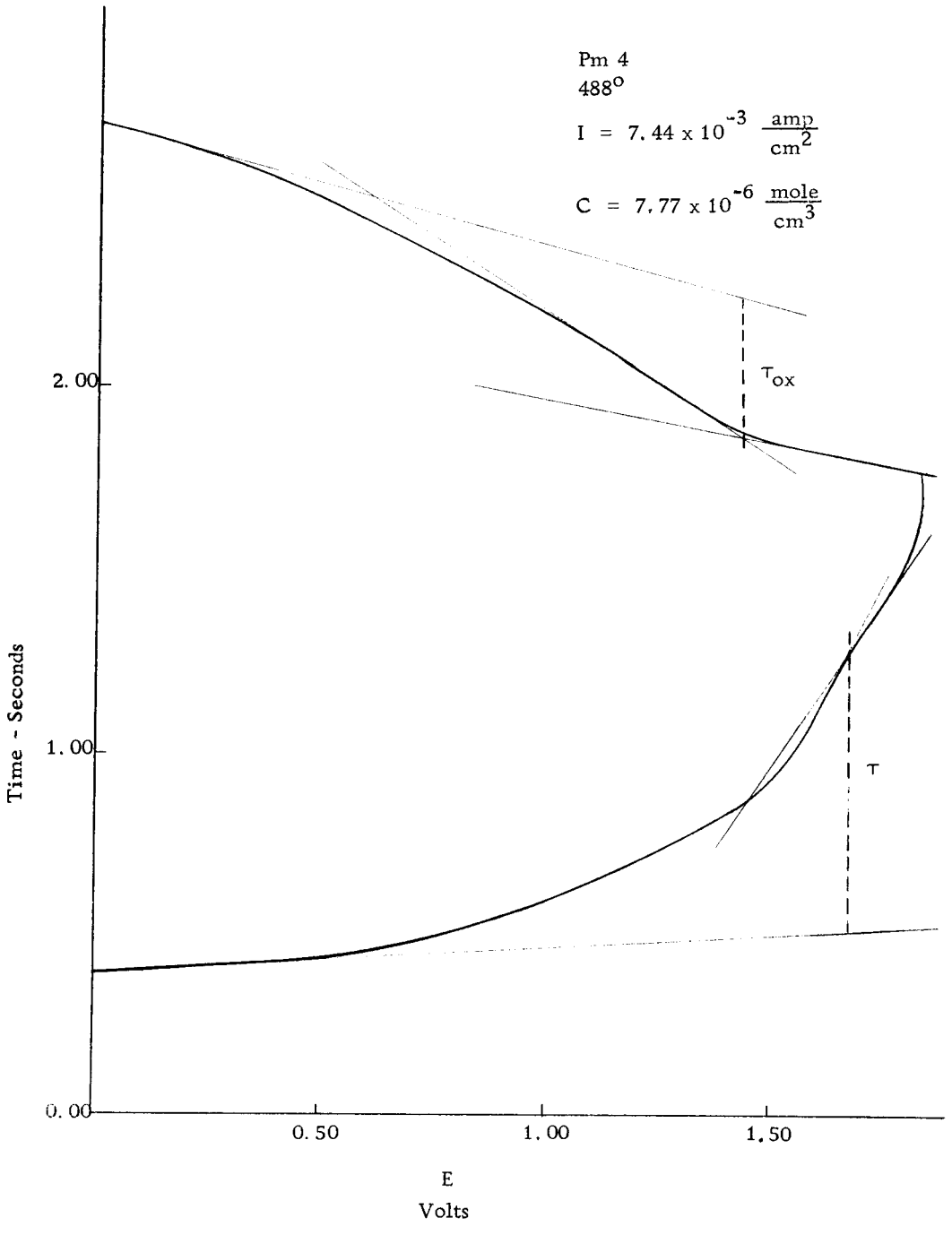

Figure 4. Chronopotentiogram of Pm(III)

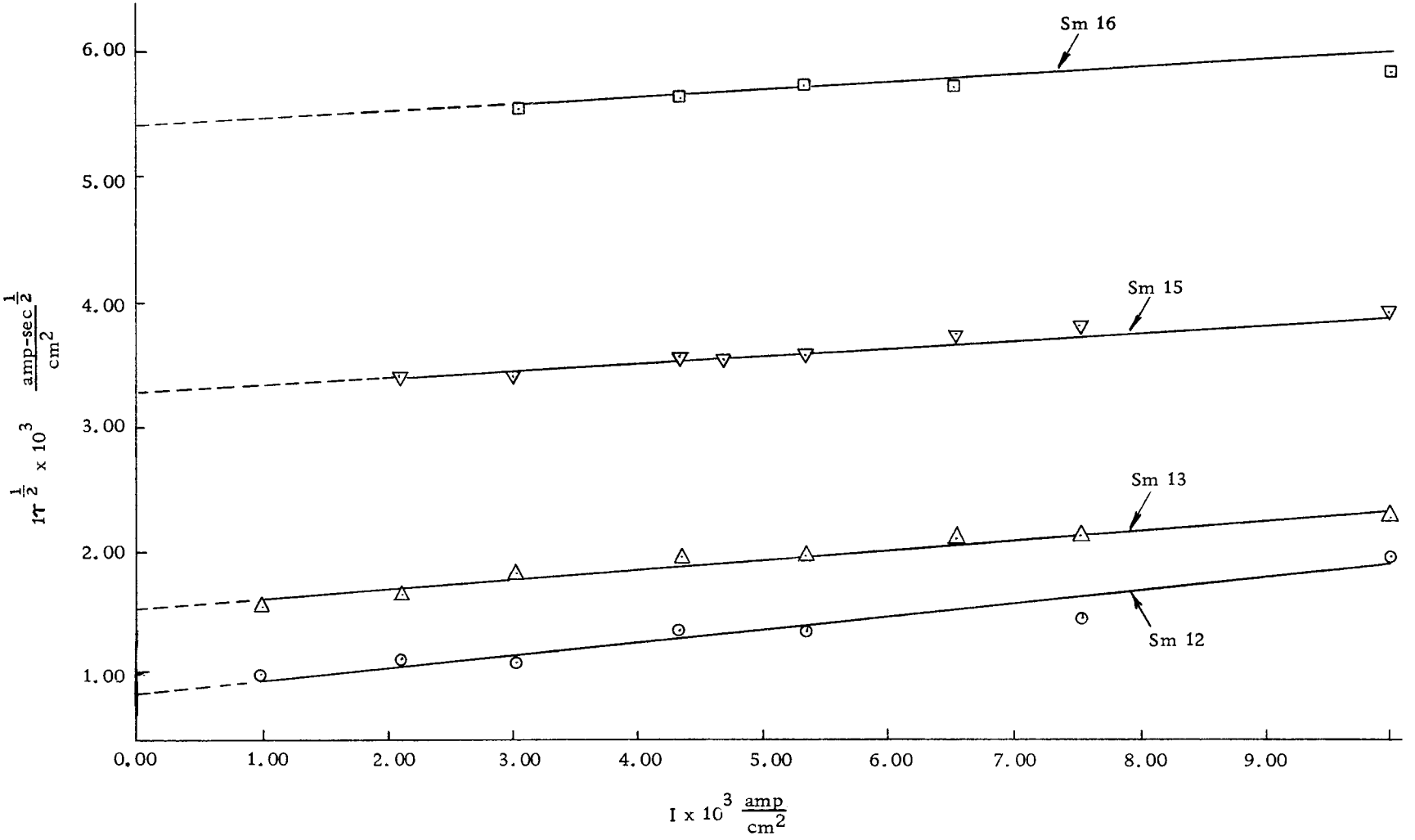

Figure 5. Graph of $I\tau^{\frac{1}{2}}$ versus I for Sm(III)

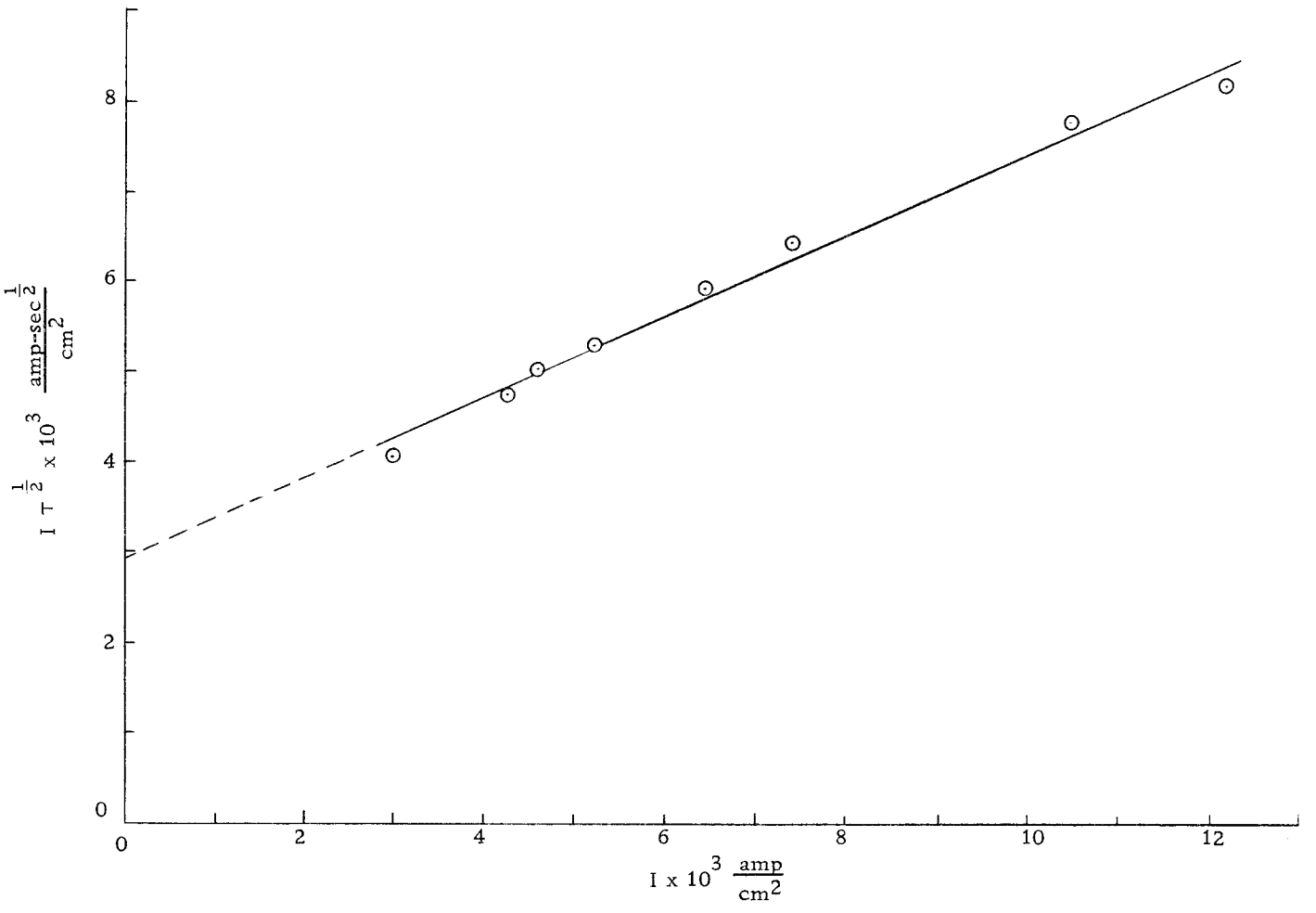

Figure 6. Graph of $I\tau^{\frac{1}{2}}$ versus I for Pm(III)

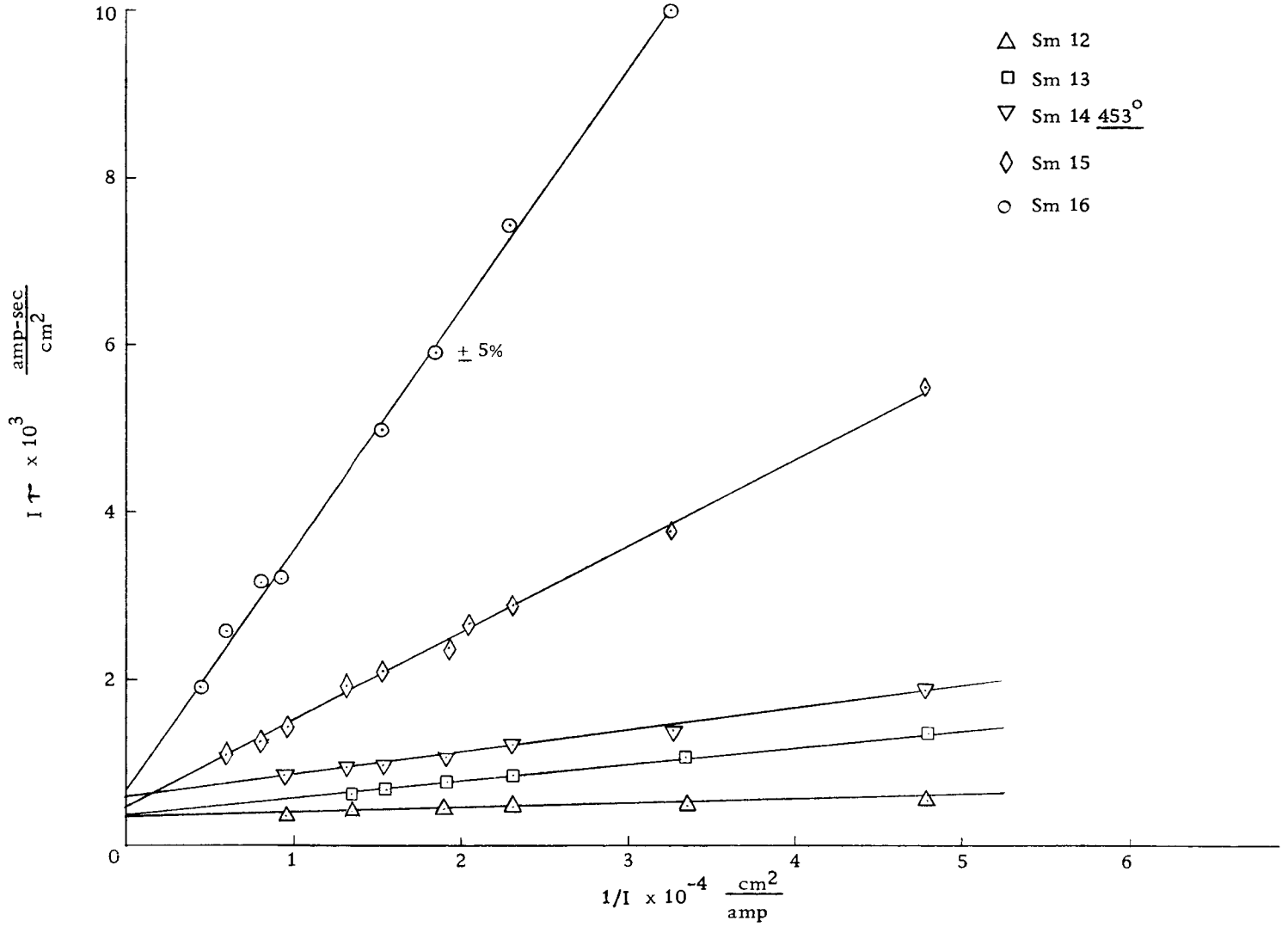

Figure 7. Graph of $I\tau$ versus $1/I$ for Sm(III)

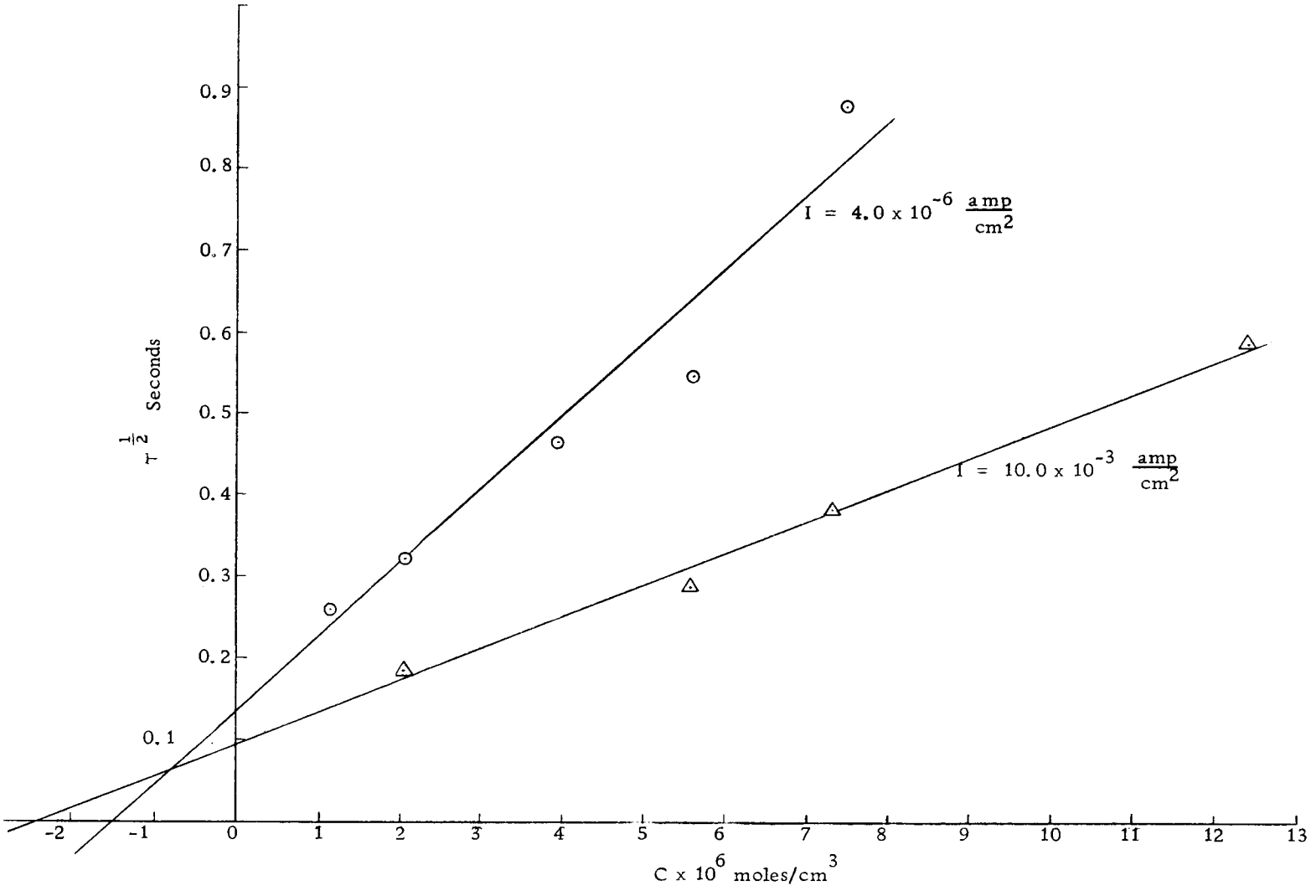

Figure 8. Graph of $\tau^{\frac{1}{2}}$ versus C for Sm(III) at constant I

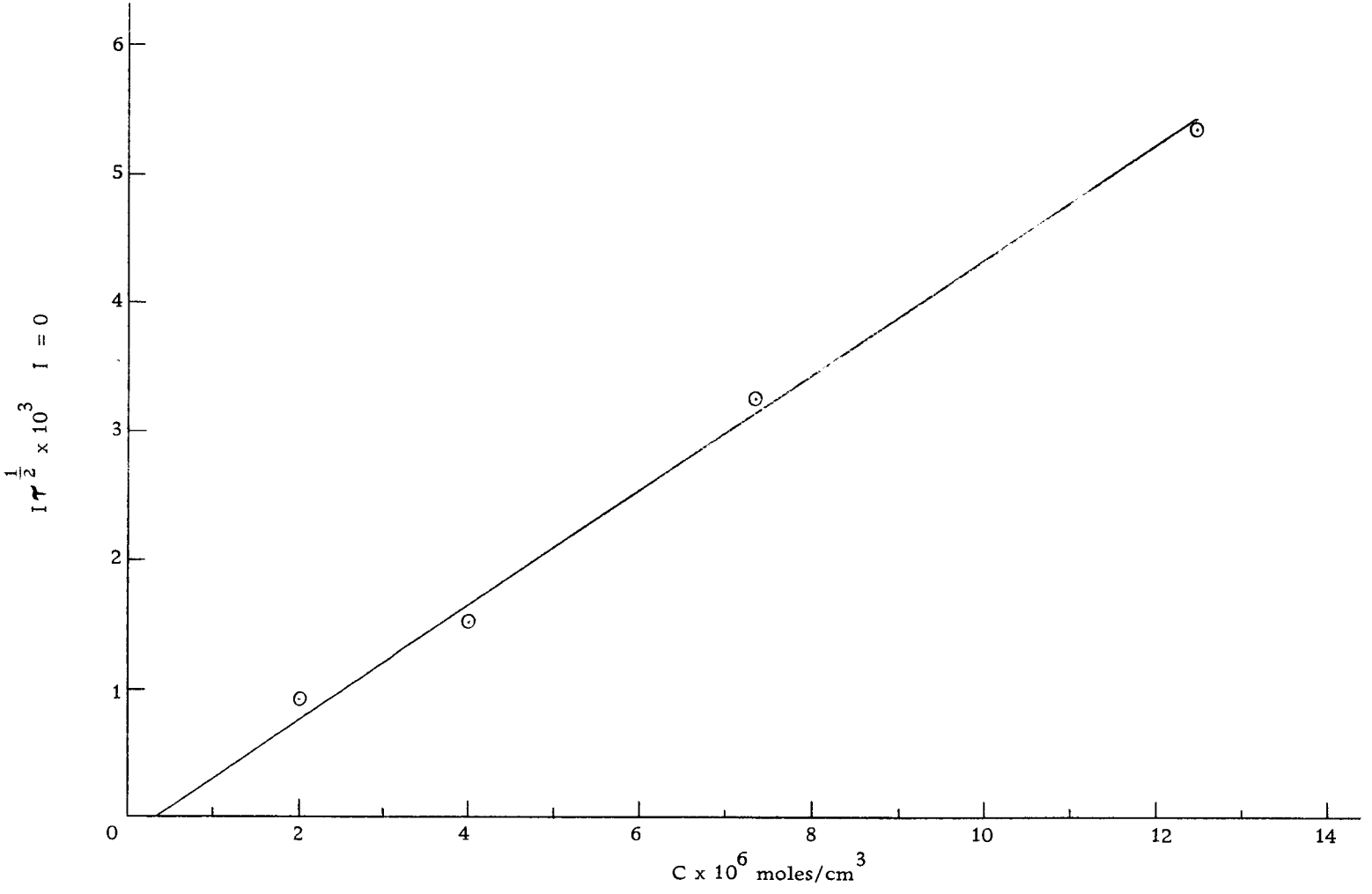

Figure 9. Graph of $I\tau^{\frac{1}{2}}$ versus C for Sm(III), at I = 0

BIBLIOGRAPHY

1. Ashley, J. W., Jr., and Charles N. Reilly. Chemical kinetics in electrochemical processes. Journal of Electroanalytical Chemistry 7:253-275. 1964.

2. Benedict, Glen E. and Richard A. Nixon. Hanford salt cycle process I. Plutonium chemistry. 1964. 19 p. (U.S. Atomic Energy Commission. HW-SA-3622)

3. Benedict, Glen E. et al. Production of reactor fuel oxides from molten chloride salt solutions. 1963. 23 p. (U.S. Atomic Energy Commission. HW-SA-2915)

4. Blander, Milton. Molten salt chemistry. New York, Interscience Publishers, 1964. 775 p.

5. Bockris, J. O'M. et al. The lifetime of complex ions in ionic liquids. Journal of Electoanalytical Chemistry 5:476-480. 1963.

6. Caja, J. and V. Pravdic. Electrochemical reduction of uranium(VI) at mercury electrodes in carbonate solutions. Journal of Electroanalytical Chemistry 8:390-398. 1964.

7. Campbell, George Melvin. A study of the third order disproportionation of divalent rare earths in molten KCl-LiCl. Use of chronopotentiometry and chemical rates. Ph. D thesis. Nashville, Vanderbilt University, 1951. 124 numb. leaves.

8. Chambers, Lee Mason. A study of adsorption by chronopotentiometry. Ph. D thesis. Urbana, University of Illinois, 1963. 90 numb. leaves.

9. Colichman, E. L. Polarography in molten ammonium formate. Analytical Chemistry 27:1559-1562. 1955.

10. Delahay, Paul. New instrumental methods in electrochemistry. New York, Interscience Publishers, 1954. 437 p.

11. Delahay, Paul and Talivaldis Berzins. Theory of electrolysis at constant current with partial or total control by diffusion. Application to the study of complex ions. Journal of the American Chemical Society 75:2486-2493. 1953.

12. Delahay, Paul and Gleb Manatov. Voltammetry at constant current. Review of fundamental principles. Analytical Chemistry 27:478-483. 1955.

13. Delimarskii, Iu. K. and B. F. Markov. Electrochemistry of fused salts. Washington, Sigma Press, 1961. 338 p. (English translation)

14. Evans, Dennis H. A study of the formation of the first electrolytic product in step-wise processes in chronopotentiometry. Journal of Electroanalytical Chemistry 9:267-275. 1965.

15. Galus, Z., H. Y. Lee and Ralph N. Adams. Triangular wave cyclic voltammetry I. Journal of Electroanalytical Chemistry 5:17-22. 1963.

16. Gaur, H. C. and R. S. Sethi. Polarography in molten salts. Journal of Electroanalytical Chemistry 7:474-486. 1964.

17. Grahme, David C. Mathematical theory of the faradaic admittance. Journal of the Electrochemistry Society 99:370c-385c. 1952.

18. Hale, J. M. The polarographic and chronopotentiometric characteristics of reversible step-wise electrode reactions. Journal of Electroanalytical Chemistry 8:181-199. 1964.

19. Hamer, Walter J., Marjorie S. Malberg and Bernard Rubin. Theoretical electromotive forces for cells containing a single solid or molten chloride electrolyte. Journal of the Electrochemistry Society 103:8-16. 1956.

20. Heal, H. G. and J. G. N. Thomas. Unstable ions of quinquevalent uranium. Transactions of the Faraday Society 45:11-20. 1949.

21. Karaglanoff, Z. Über Oxydations-und Reduktionvorgänge bei der Elektrolyse von Eisensalzlosungen. Zeitschrift für Elektrochemie 12:5-16. 1906.

22. Kolthoff, I. M. and W. E. Harris. The polarography of uranium. II. Polarography in strongly acidic solution. Journal of the American Chemical Society 68:1175-1179. 1946.

23. Kublick, Z. Cyclic voltage sweep chronoamperometry with a platinum microelectrode. Journal of Electroanalytical Chemistry 5:450-460. 1963.

24. Laitinen, H. A. and W. S Fergason. Chronopotentiometric analysis in fused lithium chloride-potassium chloride. Analytical Chemistry 29:4-9. 1957.

25. Laitinen, H. A. and H. C Gaur. Impedance and polarization measurements in fused lithium chloride-potassium chloride. Journal of the Electrochemistry Society 104:730-737. 1957.

26. Laitinen, H. A., R. P. Tischer and D. K. Roe. Exchange current measurements in KCl-LiCl eutectic melt. Journal of the Electrochemistry Society 107:546-555. 1960.

27. Lingane, James J. Electroanalytical chemistry. 2d ed. New York, Interscience Publishers, 1958. 669 p.

28. Lorenz, Wolfgang. Über den Einfluss von Oberflächenrauhigkeit und Potentialbestimmender Ionenadsorption an Elektroden auf das Anklingen der Diffusionspolarisation bei Konstantem Strom. Zeitschrift für Elektrochemie 59:730-736. 1955.

29. Morachevskii, A. G. and B. V. Patrov. Survey of research in 1963 on the electrochemistry of fused salts. Zhurnal Prikladnoi Khimii 37:1396-1408. 1964.

30. Nicholson, Richard S. and Irving Shain. Theory of stationary electrode polarography. Analytical Chemistry 36:706-723. 1964.

31. Nissen, Donald A. Electrochemistry of plutonium(III) in molten alkali chlorides. 1965. 9 p. (U.S. Atomic Energy Commission. BNWL-158)

32. Peters, Dennis G. and Stephen A. Cruser. Cathodic chronopotentiometry of copper (I) and copper (II) in chloride media. Journal of Electroanalytical Chemistry 9:27-40. 1965.

33. Randles, J.E.B. and W. White. Reactions of metal ions at mercury electrodes in fused salts. Zeitschrift für Electrochemie 59:666-671. 1955.

34. Reilly, Charles N., Grover W. Everett and Richard H. Johns. Voltammetry at constant current. Experimental evaluation. Analytical Chemistry 27:483-491. 1955.

35. Reinmuth, W. H. Chronopotentiometric potential-time curves and their interpretation. Analytical Chemistry 32:1514-1517. 1960.

36. Reinmuth, W. H. Chronopotentiometric transition times and their interpretation. Analytical Chemistry 33:322-325. 1961.

37. Reinmuth, W. H. Distortion of chronopotentiograms from double layer and surface roughness effects. Analytical Chemistry 33:485-487. 1961.

38. Roe, David Kelmer. Electrode reaction kinetics in fused potassium chloride-lithium chloride. Ph.D thesis. Urbana, University of Illinois, 1959. 73 numb. leaves.

39. Ryabulkhin, Yu. M. The influence of convection of the transition time in chronopotentiometry. Russian Journal of Physical Chemistry 37:363-364. 1963. (Translated from Zhurnal Fizicheskoi Khimii)

40. Sand, Henry J.S. On the concentration at the electrodes in a solution, with special reference to the liberation of hydrogen by the electrolysis of a mixture of copper sulphate and sulfuric acid. Philosophical Magazine, Ser. 6, 1:45-78. 1901.

41. Stromatt, Robert W. Studies on the electroreduction of uranyl (VI) in molten equimolar KCl-NaCl by chronopotentiometric and electrode impedance methods. Journal of the Electrochemical Society 110:1277-1282. 1963.

42. Sundheim, Benson R. Fused salts. New York, McGraw-Hill, 1964. 435 p.

43. Testa, A. C. and W. H. Reinmuth. Chemical kinetic parameters from chronopotentiometric potential-time measurements. Analytical Chemistry 32:1518-1520. 1960.

44. Testa, A. C. and W. H. Reinmuth. Mechanism of o-nitrophenol reduction by chronopotentiometry. Journal of the American Chemical Society 83:784-786. 1961.

45. Testa, A. C. and W. H. Reinmuth. Stepwise reactions in chronopotentiometry. Analytical Chemistry 33:1320-1324. 1961.

46. Thalmayer, C.E., S. Bruckenstein and D. M. Gruen. Chronopotentiometric determination of interdiffusion coefficients and heats of interdiffusion in molten salts. Journal of Inorganic and Nuclear Chemistry 26:347-357. 1964.

47. Tyagai, V.A. and Yu. V. Pleskov. Apparatus for electrochemical measurements using pulse techniques. Russian Journal of Physical Chemistry 38:1148-1150. 1964. (Translated from Zhurnal Fizicheskoi Khimii)

48. Van Artsdalen, E.R. Some kinetic considerations about fused salts. In: Proceedings of a symposium on High Temperature - a tool for the future, Berkeley, California, June 1956. Menlo Park, California, Stanford Research Institute, 1956. p. 133-135.

49. Van Artsdalen, E.R. and I.S. Yaffe. Electrical conductivity and density of molten salt systems: KCl-LiCl, KCl-NaCl, KCl-KI. Journal of Physical Chemistry 59:118-127. 1955.

50. Vielstich, Wolf and Paul Delahay. Voltage-step method for the kinetic sutdy of fast electrode reactions. Journal of the American Chemical Society 79:1874-1876. 1957.

51. Weber, Henry F. Untersuchungen uber des Elementargesetz der Hydrodiffusion. Wiedmann's Annalen der Physik 7:536-552. 1879.

52. Zemczuzny, S. and F. Rambach. Schmelzen der Alkali-chloride. Zeitschrift für anorganische Chemie 65:403-407. 1910.